https://doi.org/10.5194/egusphere-2025-546
Preprint. Discussion started: 13 February 2025

Retrieving Vertical Profiles of Cloud Droplet Effective Radius using Multispectral Measurements from MODIS: Examples and Limitations

Andrew J. Buggee[1,2], Peter Pilewskie[1,2]

[1]Laboratory for Atmospheric and Space Physics, Boulder, 80303, United States of America
[2]Atmospheric and Oceanic Sciences, University of Colorado Boulder, Boulder, 80303, United States of America

Correspondence to: Andrew J. Buggee (andrew.buggee@lasp.colorado.edu)

Abstract. With the coming launch of the Climate Absolute Radiance and Refractivity Earth Observatory (CLARREO) Pathfinder (CPF) comes an opportunity to develop a new cloud retrieval from spectral reflectance measurements. With continuous coverage across the shortwave spectrum and a factor of 5 to 10 lower radiometric uncertainty than the Moderate Resolution Imaging Spectroradiometer (MODIS), CPF facilitates the retrieval of a vertical profile of droplet size, providing insight into the internal structure of a cloud. Measurements from MODIS coincident with in situ observations provide the foundation for developing a constrained optimal estimation technique, ensuring a solution consistent with forward model assumptions. The limited unique information in the MODIS bands used in this analysis led to a non-unique solution, with many droplet profiles leading to convergence. Droplet size at cloud bottom is difficult to constrain because visible and near-infrared reflectances have an average penetration depth near cloud top. The region of convergence within the solution space decreased along the cloud bottom radius dimension by 2 μm when increasing the number of wavelengths used in the retrieval from seven to 35, and by 5 μm when reducing the measurement uncertainty from 2% to 0.3%. The enhanced accuracy and, to a lesser degree, the enhanced spectral sampling provided by CPF measurements are essential to extracting vertically resolved droplet size information from moderately thick, warm clouds.

1 Introduction

Clouds affect Earth's climate in complex, pivotal ways by modulating incoming and outgoing radiation. They affect weather on short time scales and climate on long time scales. In situ cloud measurements provide thermodynamic and microphysical information over small spatial scales, but the cost of scaling these observations daily and globally is prohibitive. Remote sensing of clouds from space provides the means of acquiring regional to global and seasonal to longer term information on cloud microphysics and the global distribution and evolution of water in the atmosphere. Monitoring cloud properties from space has improved our understanding of the impacts of clouds on Earth's climate but cloud feedbacks remain a critical challenge to predicting future climate states.

https://doi.org/10.5194/egusphere-2025-546
Preprint. Discussion started: 13 February 2025

Passive optical remote sensing of clouds uses measured spectral reflectance of solar radiation to retrieve cloud optical depth (the number of photon mean free paths over the vertical geometric depth of a cloud layer) and the extinction weighted cloud effective droplet radius. These cloud optical properties "…are both a consequence of and an expression for the solar radiative transfer characteristics of clouds (Stephens et al., 2019)." Cloud optical depth plays a fundamental role in cloud radiative feedbacks (Stephens, 2005), and cloud reflectivity (Bohren and Clothiaux, 2006). The effective droplet radius is linearly related to one minus the single scattering albedo, sometimes called the co-albedo, over much of the solar spectrum and can be used to approximate the fraction of light absorbed by optically thick clouds due to multiple scattering (Twomey and Bohren, 1980). From cloud optical depth and effective droplet radius, liquid water path (mass of liquid water in a column of air) and droplet number concentration (number of droplets in a unit of volume) can be derived. Liquid water path is related to cloud droplet growth processes and the onset of precipitation (Miller et al., 2016), and has been used to used verify the representation of clouds in climate models (Stephens et al., 2019). Droplet number concentration is used as a proxy for cloud condensation nuclei to study the aerosol indirect effect (Feingold et al., 2006).

Scattered solar radiation from clouds has been used to derive effective droplet radius, cloud optical thickness, and cloud phase since the 1960s. Sagan and Pollack (1967) used spectrally varying reflectance measurements to study the clouds of Venus. Hansen and Pollack (1970) applied the same techniques to terrestrial clouds using measurements taken by a near-infrared spectrometer on board a high-altitude U-2 plane. Twomey and Seton (1980) expanded on this work by outlining what is now considered the standard method for deriving cloud optical properties with spectral measurements in the visible and near-infrared. Throughout the 1980s and 1990s, several methods of reliably determining droplet size and optical depth (Nakajima and King, 1990; Twomey and Cocks, 1982) as well as cloud phase (Pilewskie and Twomey, 1987) from remote measurements were developed. Beginning in the early 2000s, the afternoon constellation of satellites, called the A-Train, put decades worth of research to the test by implementing these retrieval algorithms on a global, daily basis. The Moderate Resolution Imaging Spectroradiometers (MODIS) on the Aqua and Terra satellites have measured scattered solar radiation and emitted terrestrial radiation in discrete spectral bands for over two decades (Platnick et al., 2003). These measurements were used to derive effective cloud droplet radius, cloud optical thickness, cloud phase, liquid water path, and droplet number concentration, for which there now exists an extensive data record.

The standard method of cloud optical remote sensing can be applied to measured reflectance in as few as two spectral bands, one at a wavelength where absorption by water is negligible and the other at a wavelength where water weakly absorbs, defined by the product of droplet size and bulk absorption coefficient being much less than unity (Nakajima and King, 1990; Twomey and Cocks, 1982). Reflectance in these two spectral regions are nearly independent from one another; at non-absorbing wavelengths reflectance is proportional to cloud optical thickness, and at wavelengths where liquid water weakly absorbs reflectance is proportional to effective droplet radius. This bi-spectral method is employed to compute the MODIS Collection 6 cloud products by computing extensive lookup tables of cloud reflectance with varying solar and viewing geometry, effective

https://doi.org/10.5194/egusphere-2025-546
Preprint. Discussion started: 13 February 2025

cloud droplet radius, and cloud optical depth (Amarasinghe et al., 2017). Cloud optical depth and effective droplet radius are retrieved by calculating the minimum ℓ^2-norm, the root-sum-square, of the difference between two MODIS spectral measurements of reflectance and the lookup table estimates.

While the bi-spectral method is straightforward to implement, it assumes that droplet size within the pixel under observation is vertically and horizontally homogenous (Amarasinghe et al., 2017). Theoretical analysis of warm, non-precipitating adiabatic clouds predicts a vertical structure of droplet size that increases from cloud base to cloud top (Yau and Rogers, 1996). Many in situ measurements of warm, non-precipitating clouds have verified this prediction; the opposite behavior has been found in precipitating clouds and clouds containing drizzle (King et al., 2013; Miles et al., 2000; Painemal and Zuidema, 2011). King et al. (2013) suggested that the assumptions within the MODIS cloud products algorithm for warm, non-precipitating clouds may lead to an overestimation of liquid water path by as much as 25%.

The bi-spectral retrieval method results in a wavelength-dependent effective radius due to the variability of liquid (and ice) water absorption in the near-infrared. This was explained by Platnick (2000) who showed that photons at different wavelengths penetrate to different depths within clouds due to the spectral dependence of single scattering albedo. Thus, the retrieved droplet radius represents a weighted average over the vertical extent of the cloud, with the largest weighting occurring at cloud top (Platnick, 2000). Following this result, Chang and Li (2002) proposed using MODIS measurements at three near-infrared spectral bands to retrieve the vertical dependence of effective droplet radius. Their method assumed a linear relationship between effective droplet radius and cloud depth, and, like MODIS Collection 6, they computed lookup tables of reflectance at each wavelength to retrieve a droplet profile. Subsequent analysis by (Chang and Li, 2003) used MODIS measurements to solve for the effective droplet radius at cloud top and bottom using a pair of near-infrared wavelengths. Repeating this for a different pair of near-infrared wavelengths, the authors retrieved a droplet profile by taking an average of the two linear retrievals. The authors concluded that creating lookup tables for more than two wavelengths and at least six free variables was too memory-intensive for practical use with real data (Chang and Li, 2003). Using the method outlined by Chang and Li (2003), Chen et al. (2007) suggested the vertical structure of droplet size can be used to discern between clouds with and without precipitation-sized droplets.

Kokhanovsky and Rozanov (2012) defined the mathematical framework for applying an optimal estimation technique to infer a vertical droplet profile using spectral measurements. They showed that four MODIS wavelengths could be used simultaneously with less computational cost than the lookup table method to solve for three variables: the effective radii at cloud top and cloud bottom and cloud optical depth. The authors demonstrated their method with synthetic and real MODIS measurements. Coddington et al. (2012) computed the gain of Shannon information content with respect to the retrieval of effective droplet radius and cloud optical depth using hundreds of measurements across the solar spectrum. The authors found that beyond the traditional method of using two wavelengths, there is additional information within 100 spectral measurements

https://doi.org/10.5194/egusphere-2025-546
Preprint. Discussion started: 13 February 2025

that can meaningfully alter the retrieval of droplet size and optical depth. King and Vaughan (2012) applied an optimal estimation technique to hundreds of synthetic spectral measurements throughout the visible and near-infrared. The use of synthetic data enabled a systematic study of the impact of measurement uncertainty on the retrieval uncertainty of cloud optical depth and the effective radii at cloud top and cloud bottom. King and Vaughan (2012) concluded that a measurement uncertainty of 1% would result in a retrieval uncertainty of less than 2 μm for the effective radius at cloud bottom and less than 0.1 μm at cloud top. It's important to note that this result depends on cloud optical depth (King and Vaughan, 2012). For the retrieved radius at cloud bottom, the authors found the minimum retrieval uncertainty for an optical depth of 10 (King and Vaughan, 2012).

The Climate Absolute Radiance and Refractivity Earth Observatory (CLARREO) Pathfinder (CPF) is an upcoming space-borne hyperspectral imaging spectrometer that will make measurements of scattered radiation contiguously between 350 to 2300 nm with a radiometric uncertainty of 0.3% (Shea et al., 2020). We have developed new methods that utilize the enhanced radiometric accuracy and spectral sampling of CPF to retrieve vertical profiles of cloud droplet size. The research herein builds upon previous studies in several ways. First, we suggest a different form of the optimal estimation technique that constrains the set of possible solutions by maintaining a retrieved droplet profile consistent with the forward model assumptions. Second, we apply this constrained optimal estimation method to MODIS data coincident in time and space with in situ measurements from the Variability of the American Monsoon Systems Ocean-Cloud-Atmosphere-Land Study Regional Experiment (VOCALS-REx) field campaign to provide a means of validation (Wood et al., 2011). For decades, researchers have investigated the inherent challenges with comparing in situ measurements and remote retrievals (Feingold et al., 2006; Nakajima et al., 1991; Painemal and Zuidema, 2011; Platnick and Valero, 1995; Stephens and Tsay, 1990; Twomey and Cocks, 1982). We discuss how comparisons between in situ and remote measurements provide support for algorithmic development, but differences in sampling volumes reveal substantial limitations. Lastly, we demonstrate how improved radiometric accuracy and, to a lesser degree, an increase in the number of spectral measurements used in the constrained retrieval decreases the set of acceptable solutions. For this analysis, we simulated top-of-atmosphere reflectance spectra sampled by the Earth surface Mineral dust source InvesTigation (EMIT) imaging spectrometer (Green et al., 2020). With 285 contiguous spectral channels from 380 to 2500 nm, the EMIT instrument acts as a surrogate for the upcoming CPF instrument (Thompson et al., 2024).

Section 2 provides an overview of passive optical remote sensing of clouds from space, reviews current methods of deriving cloud optical properties from satellite measurements, and introduces the constrained optimal estimation method used in this analysis. Section 3 describes the data and forward model assumptions. Section 4 presents results with comparisons between the retrieved vertical profiles and the in situ data and highlights the dependence on radiometric accuracy. Section 4 also discusses challenges comparing in situ and remote measurements and the effects of increasing the number of wavelengths used in the retrieval. Section 5 provides an interpretation of the results and discusses potential future work to improve the methods.

https://doi.org/10.5194/egusphere-2025-546
Preprint. Discussion started: 13 February 2025

2 Passive Optical Remote Sensing of Clouds

2.1 The Standard Method

Deriving cloud optical properties from spectral reflectance measurements constitutes an inverse problem. As with any inverse problem, the solutions are highly dependent on the assumptions made in the forward model. When setting up a retrieval of cloud effective radius and cloud optical depth, the fundamental question is: What combination(s) of these variables would lead to the set of observations measured? Let $\boldsymbol{x}$ be the state vector that contains the variables we seek to retrieve, thus $\boldsymbol{x} = (r_e, \tau_c)$. To solve for $\boldsymbol{x}$, we define a forward model, R, which maps our state vector to a set of spectral reflectance measurements, $\boldsymbol{m}$, such that $R(\boldsymbol{x}) = \boldsymbol{m}$. The relationship between the desired state vector and spectral reflectance is non-linear.

The MODIS collection 6 cloud retrieval uses the bi-spectral method, relying on an extensive library of forward model calculations to retrieve the effective droplet radius, r_e, and cloud optical depth, τ_c (Platnick et al., 2017). The effective radius is defined mathematically as the ratio of the third moment of the droplet size distribution, $n(r)$, to the second moment (Hansen and Travis, 1974):

$$r_e = \frac{\int_0^\infty r\,\pi\,r^2\,n(r)\,dr}{\int_0^\infty \pi\,r^2\,n(r)\,dr} \tag{1}$$

In addition to the desired state vector, each reflectance calculation depends on the solar and viewing geometry, the surface albedo, wavelength, and molecular and aerosol scattering and absorption. Note that these independent variables are not included in our equations. Lookup tables are created by computing reflectance over ranges of each these independent variables. The desired variables r_e and τ_c are determined by computing the minimum ℓ^2-norm difference between the measured reflectances, $\boldsymbol{m}$, and the forward model estimates of reflectance, $R(\boldsymbol{x})$.

2.2 Monte Carlo Derived Weighting Functions

Unless droplet size is uniform throughout a cloud, the bi-spectral retrieval of effective radius depends on the two wavelengths chosen because average photon penetration depth within a cloud depends on the wavelength-dependent single scattering albedo (Platnick, 2000). Using a Monte Carlo model, we derived the weighting functions for the first seven spectral channels of MODIS to determine the average penetration depth for a vertically inhomogeneous cloud. A Monte Carlo model can simulate radiative transfer by treating photon-particle interactions stochastically. The critical element of this model is to define the processes of scattering and absorption probabilistically and then map each of these distributions onto a uniform probability distribution that can be sampled with a random number generator.

https://doi.org/10.5194/egusphere-2025-546
Preprint. Discussion started: 13 February 2025

Clouds were modelled as horizontally infinite plane-parallel layers with a finite optical thickness and a vertical profile of effective radius. Liquid water content, LWC, is defined as the total mass of liquid water per unit volume of air:

$$LWC = \int_0^\infty \rho \frac{4}{3} \pi\, r^3\, n(r)\, dr \tag{2}$$

where ρ is the density of liquid water. Assuming a parcel of air rises adiabatically, LWC increases linearly with geometric height. A linear relationship between liquid water content and height can be defined as:

$$LWC(z) = LWC(0) + \big(LWC(H) - LWC(0)\big) \frac{z}{H} \tag{3}$$

where H is the total geometric depth of the cloud such that $z = 0$ at cloud base and $z = H$ at cloud top. If we assume that total number concentration, $N_c(z)$, is constant with height, and we define the droplet distribution as consisting of a single radius, r_e, then we can remove the integral in Eq. (2) and use Eq. (3) to solve for the effective radius under the adiabatic assumption:

$$r_e(z) = \left(\frac{3}{4\pi N_c\, \rho}\, (LWC(0) + (LWC(H) - LWC(0)) \frac{z}{H}))\right)^{\frac{1}{3}} = (r_{bot}^3 + \, (r_{top}^3 - r_{bot}^3\,) \frac{z}{H})^{\frac{1}{3}} \tag{4}$$

where r_{top} and r_{bot} are the effective radii at cloud top and cloud base, respectively (Platnick, 2000). This droplet profile was used for the Monte Carlo simulations. Clouds were comprised of 100 plane-parallel layers with droplet size following a narrow gamma distribution in each layer (Deirmendjian, 1964). Figure 1 shows normalized weighting functions for a vertically inhomogeneous cloud. Each weighting function represents the conditional probability of a photon scattered in the upward direction at cloud top, given that it penetrated to a max depth of τ.

The wavelength-dependent column-weighted effective radius is:

$$r_e^* = \int_0^{\tau_c} r_e(\tau)\, w_\lambda(\tau)\, d\tau \tag{5}$$

where $w_\lambda(\tau)$ is the wavelength-dependent weighting function (Platnick, 2000). For a non-constant droplet profile, Eq. (5) represents the retrieved effective radius for a given wavelength. From Fig. 1, it is evident that reflectance at different near-infrared wavelengths depend on the droplet profile. Since single scattering albedo, ϖ_0, and to a lesser extent the asymmetry parameter, varies with wavelength, measurements at different wavelengths probe different depths within a cloud. In general, droplet absorption, defined by $1 - \varpi_0$, controls the vertically dependent weighting functions since photons that are more likely

https://doi.org/10.5194/egusphere-2025-546
Preprint. Discussion started: 13 February 2025

to be absorbed are less likely to penetrate deep into cloud layers. Figure 1 shows that on average, reflectance is dominated by scattering from the cloud top due to a greater proportion of photons reaching a maximum penetration depth in the upper region of the cloud.

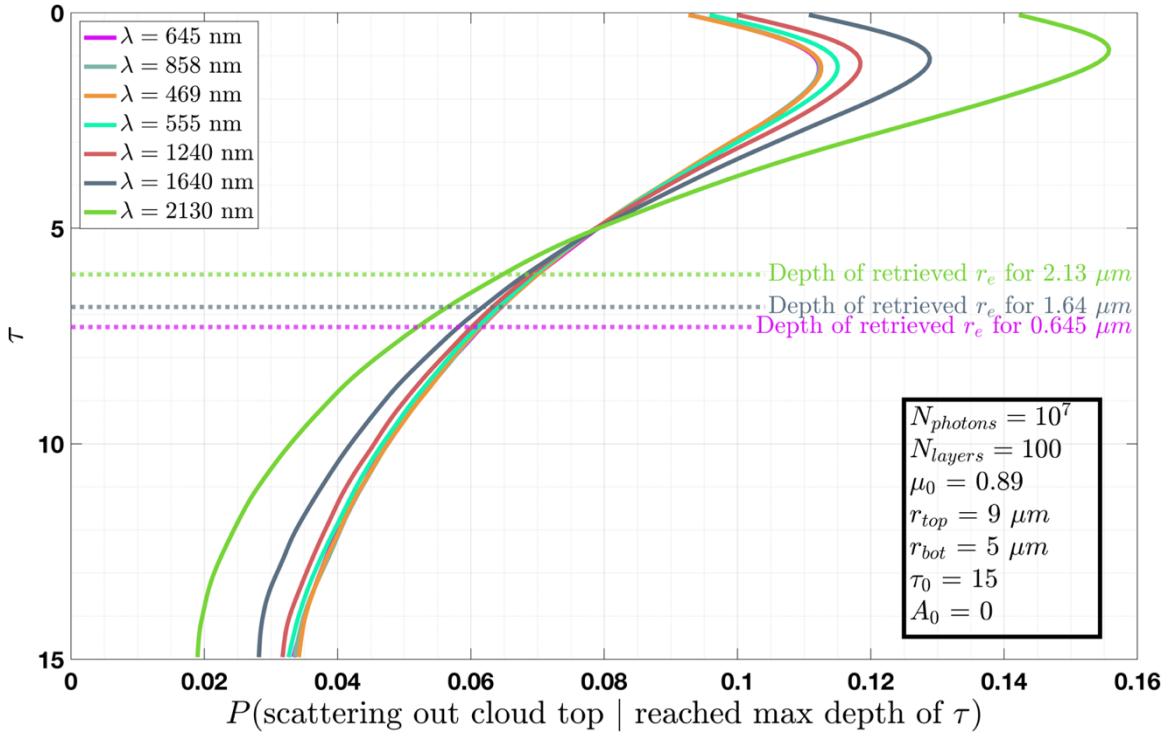

Figure 1: Weighting functions of the MODIS instrument's first seven spectral channels. Model parameters are shown in the lower right corner. μ_0 is the cosine of the solar zenith angle, A_0 is the surface albedo below the cloud layer, $N_{photons}$ represents the number of photons used to compute each weighting function, N_{Layers} represents the number of homogeneous, plane-parallel layers, and τ_0 is the total optical depth of the cloud. Horizontal dashed lines represent the optical depth associated with the retrieved effective radius using the wavelength specified (Eq. (5)).

The development of a Monte Carlo simulation to model radiative transfer within clouds provided insight into how wavelength-dependent reflectance samples different layers of clouds. If r_e were constant with height the structure of each weighting function and the depth of average penetration would be irrelevant. Figure 1 shows that weighting functions at all seven MODIS wavelengths used in this analysis reach a similar maximum optical depth of about one. Furthermore, these weighting functions are broad and have considerable overlap, signifying considerable correlation between reflectances at different wavelengths. Ideally, a set of orthogonal weighting functions that probe different depths of the cloud would be preferred. While this is not achieved with wavelengths in the visible and near-infrared region, measurements at many wavelengths can still be used to increase the retrieval signal-to-noise ratio.

2.3 The Constrained Optimal Estimation Method

https://doi.org/10.5194/egusphere-2025-546
Preprint. Discussion started: 13 February 2025

Kokhanovsky and Rozanov (2012) applied an optimal estimation technique to retrieve a state vector that included droplet size at cloud top and base: $\boldsymbol{x} = (r_{top}, r_{bot}, \tau_c)$. Importantly, this technique requires an assumption about the dependence of droplet size with altitude within cloud. Once droplet size is retrieved at the top and base, $r_e(\tau)$ can be determined continuously across the domain $\tau = [0, \tau_c]$. We assumed the droplet profile was adiabatic according to Eq. (4).

The Gauss-Newton iterative method, a technique used to solve non-linear least-squares problems, is used to solve for the state vector (Rodgers, 2000). At each iteration, the new state vector estimate is:

$$\boldsymbol{x}_{i+1} = \boldsymbol{x}_i + (\mathbf{S}_a^{-1} + \mathbf{K}_i^T\ \mathbf{S}_\epsilon^{-1}\ \mathbf{K}_i)^{-1}\ [\mathbf{K}_i^T\ \mathbf{S}_\epsilon^{-1}\ (\boldsymbol{m} - R(\boldsymbol{x}_i)) + \mathbf{S}_a(\boldsymbol{x}_i - \boldsymbol{x}_a)] \quad (6)$$

where matrices are indicated in capitalized boldface, and vectors are indicated in lowercase, italicized boldface. $\boldsymbol{x}_i$ is the state vector estimate of the i^{th} iteration, $\boldsymbol{x}_a$ is the a priori state vector, $\mathbf{S}_a$ is the a priori covariance matrix, $\mathbf{K}_i$ is the Jacobian matrix of $R(\boldsymbol{x}_i)$, and $\mathbf{S}_\epsilon$ is the measurement covariance matrix. The a priori state vector represents the best guess of the values of each retrieved variable before the Gauss-Newton iterative solution is derived. The a priori covariance matrix accounts for the uncertainty in the a priori guess and the relationship between each state variable. Likewise, the measurement covariance matrix defines the measurement uncertainty at each wavelength and the correlation between measurements at different wavelengths. Two measurements with a non-zero covariance are at least partially redundant with respect to retrieving the desired variables. The Jacobian is defined as:

$$\mathbf{K_i} = \nabla R(\boldsymbol{x}_i) = \begin{bmatrix} \frac{\partial R(\boldsymbol{x}_i,\lambda_1)}{\partial r_{top}} & \frac{\partial R(\boldsymbol{x}_i,\lambda_1)}{\partial r_{bot}} & \frac{\partial R(\boldsymbol{x}_i,\lambda_1)}{\partial \tau_c} \\ \frac{\partial R(\boldsymbol{x}_i,\lambda_2)}{\partial r_{top}} & \frac{\partial R(\boldsymbol{x}_i,\lambda_2)}{\partial r_{bot}} & \frac{\partial R(\boldsymbol{x}_i,\lambda_2)}{\partial \tau_c} \\ \cdots & \cdots & \cdots \end{bmatrix} \quad (7)$$

The forward model, R, is used to compute reflectance at a set of wavelengths for some cloud state, $\boldsymbol{x}_i$. The Jacobian represents the change in reflectance due to a perturbation in each state variable. Equation 6 balances several competing factors during each iteration: the difference between the measured and computed reflectances ($\boldsymbol{m} - R(\boldsymbol{x}_i)$), the difference between the current state estimate and the a priori ($\boldsymbol{x}_i - \boldsymbol{x}_a$), and the rate of change of the estimated measurements with respect to the current state variable ($\mathbf{K}_i = \nabla R(\boldsymbol{x}_i)$).

To construct Eq. (7), we compute the change in reflectance due to a small change in one of the state variables. For example:

https://doi.org/10.5194/egusphere-2025-546
Preprint. Discussion started: 13 February 2025

$$\frac{\partial R(\boldsymbol{x}_i,\lambda_1)}{\partial r_i^{top}} \approx \frac{\Delta R\left((r_i^{top}+\Delta r^{top}, r_i^{bot}, \tau_{c_i}),\lambda_1\right)}{\Delta r^{top}} \tag{8}$$

is the change in reflectance due to a change in the radius at cloud top. We defined the change in the state variables as a fraction of the current iteration state vector. However, the magnitude of the change in reflectance depends on the initial values of the state variables. In addition, we need the change in reflectance to be greater than the measurement uncertainty. To ensure these conditions for all cases analyzed, the Jacobian was computed using the following fractions to estimate the partial derivatives: $\Delta \boldsymbol{x}_i = \left[0.1 r_i^{top},\ 0.35 r_i^{bot}, 0.1\tau_{c_i}\right]$. These values, determined through trial and error, ensured that the reflectance change exceeded the measurement uncertainty when the state vector was outside of a local minimum.

During our analysis, we determined a need to constrain the solution space of the retrieved variables when using the Gauss-Newton iterative technique. We adopted the bound-constraint method by Doicu et al. (2003) to ensure the following constraints were satisfied:

$$\begin{aligned} &r_{bot} < r_{top} \\ &1 < r_{bot} < 25 \\ &1 < r_{top} < 25 \end{aligned} \tag{9}$$

If the first constraint is not satisfied, the forward model assumption is invalidated. The second and third constraints are required due to the range of pre-computed Mie calculations used by libRadtran (Emde et al., 2016). For each iteration, we defined a new direction as:

$$\boldsymbol{p}_i = (\mathbf{S}_a^{-1} + \mathbf{K}_i^T\ \mathbf{S}_\epsilon^{-1}\ \mathbf{K}_i)^{-1}\ [\mathbf{K}_i^T\ \mathbf{S}_\epsilon^{-1}\ (\boldsymbol{m} - R(\boldsymbol{x}_i)) + \mathbf{S}_a(\boldsymbol{x}_i - \boldsymbol{x}_a)] \tag{10}$$

such that the updated state vector guess was: $\boldsymbol{x}_{i+1} = \boldsymbol{x}_i + \boldsymbol{p}_i$ (Doicu et al., 2003). We then solved for the maximum scaler value, a, that resulted in a new state vector, $\boldsymbol{x}_{i+1} = \boldsymbol{x}_i + a\boldsymbol{p}_i$, that met our state variable constraints and resulted in a lower ℓ^2-norm between the estimate and true measurements:

$$\sqrt{\sum(R(\boldsymbol{x}_i + a\boldsymbol{p}_i) - \boldsymbol{m})^2} < \sqrt{\sum(R(\boldsymbol{x}_i) - \boldsymbol{m})^2} \tag{11}$$

from hereon we will use the term residual to refer to the left side of Eq. (11), the ℓ^2-norm of the difference between the forward model reflectances and the true measurements. This was repeated until one of two convergence metrics was met. If the percent difference of the residual between two successive iterations was less than 3%, the process was terminated. This value was

https://doi.org/10.5194/egusphere-2025-546
Preprint. Discussion started: 13 February 2025

adopted from an extensive number of retrievals. Values lower than 3% were the result of a local minima and further iterations never led to significant changes in the retrieved state vector. The other convergence criteria terminated the iterative process if the residual was less than or equal to the ℓ^2-norm of the measurement uncertainty and the previous iteration (Doicu et al., 2003):

$$\sqrt{\sum(R(\boldsymbol{x}_{i+1}) - \boldsymbol{m}\ )^2} \leq \sqrt{\sum(\delta \boldsymbol{m})^2} < \sqrt{\sum(R(\boldsymbol{x}_i) - \boldsymbol{m}\ )^2} \tag{12}$$

Once convergence occurred, the posterior covariance matrix was computed. The uncertainties of the retrieved variables are the square root of the main diagonal (Rodgers, 2000).

3 Data Used and Forward Model Assumptions

In this analysis, libRadtran (Emde et al., 2016) was used to run 1D DISORT (Stamnes et al., 2000) to compute forward modeled spectral reflectance. All clouds were defined as they were in the Monte Carlo simulations (Sect. 2.2) with an adiabatic droplet profile, 100 plane-parallel layers and a gamma droplet distribution. For all simulations shown, the distribution width parameter, α, was set to 10 based on analysis of in situ measurements of non-precipitating marine stratocumulus clouds from the VOCALS-REx flight campaign. We used the MODIS retrieval of cloud top height to define the upper boundary of the cloud. Cloud geometric thickness was set to 0.5 km, following a similar approach as the MODIS Cloud Products retrieval algorithm and our own analysis showing negligible impacts of cloud geometric thickness on reflectance for the wavelengths used. It is worth noting that, while an accurate forward model is desired, the primary function of the forward model and algorithm developed for this research was a proof-of-concept for retrieving vertical droplet profiles. Future iterations of this algorithm will continue to improve the accuracy of our forward model.

During VOCALS-REx, aircraft measurements of cloud droplet profiles were acquired from 14 flights conducted from 15 October to 15 November 2008. Some of the flight paths were spatially and temporally coincident with overpasses of the Terra and Aqua satellites (Wood et al., 2011). Over the entire duration of VOCALS-Rex, three vertical profiles were sampled within 5 minutes of a MODIS overpass, providing the best opportunities for comparison with remote retrievals. The Cloud Droplet Probe (CDP) manufactured by Droplet Measurement Technologies (Lance et al., 2010) measured forward scattering from a laser source to determine droplet diameters between 2 and 52 μm. The two-dimensional cloud optical array probe (2DC) by Particle Measurement Systems (Strapp et al., 2001) similarly measured droplet diameters between 25 and 1560 μm. To avoid redundancy, we ignored the 2DC data for droplet diameters less than 52 μm. These two data sets are distinct in that one consists primarily of typical cloud droplet sizes (~10 μm), whereas the other contains drizzle and precipitation-sized droplets (>100 μm). These two measurement systems enabled us to segregate clouds between those with and without drizzle by using a liquid

https://doi.org/10.5194/egusphere-2025-546
Preprint. Discussion started: 13 February 2025

water path threshold of 1 $g\ m^{-2}$ as measured by the 2DC instrument, a slightly lower threshold than was used by Painemal and Zuidema (2011). This effectively removed any sampled clouds with droplets larger than 52 μm from our data set. Painemal and Zuidema (2011) found a positive bias for the CDP LWC measurements compared to those from a hot wire probe. We applied their prescribed correction using a simple linear regression to the CDP droplet size distribution. In defining cloud top and bottom within the in situ data, we followed Painemal and Zuidema (2011), who defined the minimum liquid water content threshold of 0.03 $g\ m^{-3}$and a minimum total droplet number concentration threshold of 1 cm^{-3}. Therefore, the cloud top and bottom were identified as the minimum and maximum altitudes where both criteria were satisfied.

Table 1: First seven spectral channels of the MODIS instrument (King et al., 1992)

Band	Bandwidth (nm)
1	620 - 670
2	841 - 876
3	459 - 479
4	545 - 565
5	1230 - 1250
6	1628 - 1652
7	2105 - 2155

Figure 2 shows the median vertical profiles of effective radius, liquid water content, and number concentration for over 100 in situ samples without drizzle or precipitation-sized droplets during VOCALS-REx. The effective radius and liquid water content followed log-normal distributions, whereas the droplet number concentrations were Gaussian distributed. The median profiles of effective radius and liquid water content closely resemble the theoretical adiabatic profiles overlaid in black. Figure 2 demonstrates that the median profile of droplet effective radius was found to increase with altitude within cloud. We found the median effective radius at cloud top was about 37% larger than the value at cloud base for non-precipitating marine stratocumulus. These results justify the adiabatic assumption that results in a linear increase in liquid water content with altitude within cloud. We also note that the median profile of droplet number concentration is roughly constant with altitude, another assumption in the forward model. We applied our constrained optimal estimation algorithm outlined in Sect. 2.3 to real data using multispectral measurements of reflectance from the first seven spectral channels of MODIS (Table 1). These seven spectral channels were used because they deliberately avoid water vapor absorption, simplifying the forward model.

The Gauss-Newton method assumes a Gaussian prior with symmetric uncertainty about the a priori value. A priori uncertainty for the cloud top radius and optical depth was set to their respective MODIS collection 6 bi-spectral retrieval uncertainties. For the a priori uncertainty of the radius at cloud bottom, we scaled the bi-spectral retrieval uncertainty of effective radius using the weighting function for 2.13 μm. For the example cloud in Fig. 1, which has a similar droplet profile as the median

https://doi.org/10.5194/egusphere-2025-546
Preprint. Discussion started: 13 February 2025

effective radius profile found during the VOCALS-Rex campaign (Fig. 2), over 50% of the measured signal comes from the upper quartile of the cloud. Only 8% of the total signal comes from the lowest quartile. Thus, we adopted a cloud bottom uncertainty of a factor 6 larger than retrieved effective radius uncertainty. The measurement covariance matrix, $\mathbf{S}_\epsilon$, was defined using the measurement uncertainty for the seven spectral channels of MODIS used in this analysis. The different spectral measurements and the retrieved variables were assumed to be independent from one another. While the use of diagonal covariance matrices is common (King and Vaughan, 2012; Kokhanovsky and Rozanov, 2012), it does not reflect the true nature of the problem (see Sect. 5).

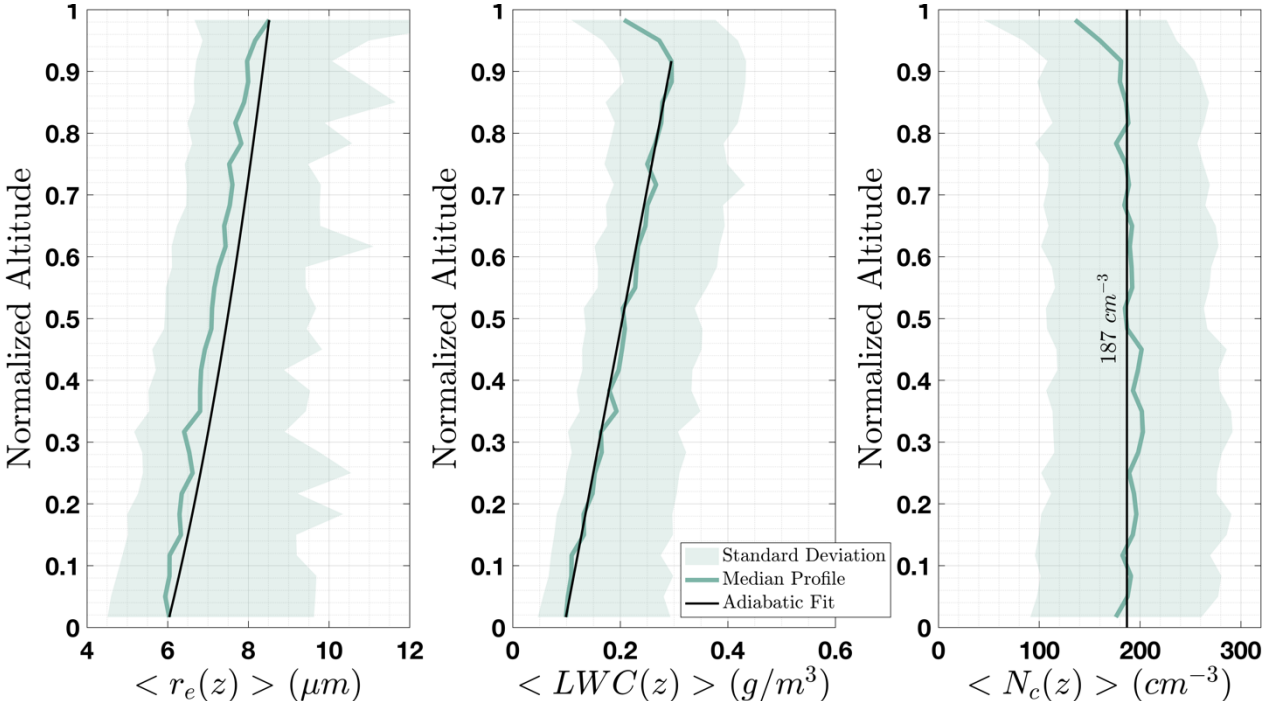

Figure 2: Median vertical profiles of effective radius, liquid water content, and droplet number concentration for non-precipitating clouds measured during the VOCALS-Rex flight campaign. The green line shows the median value of the distribution as a function of normalized cloud depth. The green-shaded area represents the average deviation above and below the median line. The black lines in the left and middle panels show the theoretical adiabatic profile using the boundary values found by the median profile. The vertical line in the right panel highlights the near-constant number concentration.

Section 4 shows retrievals for the three vertical profiles sampled within 5 minutes of a MODIS overpass. To account for the temporal displacement of cloud location, we applied a simple advection model using horizontal wind speed and direction measured on the aircraft. Using the median wind speed and direction from within the cloud, we computed the distance the cloud would have travelled during the time between MODIS and VOCALS-REx. The location was either projected forward or backward depending on whether the in situ sampling occurred before or after the MODIS overpass. The horizontal distance travelled by plane during in situ sampling exceeded the MODIS pixel sampling distance for all cases show in this paper. None

https://doi.org/10.5194/egusphere-2025-546
Preprint. Discussion started: 13 February 2025

of the droplet profiles shown in Sect. 4 were contained within a single pixel. After applying our advection model, the MODIS pixel closest to the newly projected location was used for the retrieval.

It is important to quantify the uncertainty of the in situ measurements since they were used to validate our retrieval algorithm. However, the CDP droplet size uncertainty estimate is attributed to several factors that make it difficult to quantify (Lance et al., 2010). Droplets that pass through the edges of the sampling area tend to have much higher uncertainty than droplets that pass through the center. Uncertainty due to coincidence, where multiple droplets pass through the sampling area within the sampling time of the detecting optics, is challenging to estimate because it depends on droplet size, particle concentration, and transit location within the sampling area. There are also limitations to the size resolution of the instrument due to the non-monotonic relationship between droplet size and the scattered laser light signal (Lance et al., 2010). Lance et al. (2010) used a water droplet generating system to determine the sizing accuracy of the CDP instrument. Using their results, we simplified the CDP measurement uncertainty for this analysis by defining an uncertainty of 20% for effective radii below 5 μm, and an uncertainty of 10% for those above 5 μm.

4 Results

Figures 3a, 3b, and 3c, show results applying the algorithm described in Sect. 2.3 for the retrievals of $r_e(\tau)$ for clouds with optical depths of 6.5, 11, and 19.5, respectively. Each figure also shows the MODIS Collection 6 bi-spectral retrieval of r_e and τ_c using measurements of 0.55 μm and 2.1 μm. The bi-spectral retrieval of effective radius is within range of the cloud top in situ measurement for each case, validating its use as the a priori value for the radius at cloud top. The estimated liquid water path from the retrieved profile was closer to the in situ measured value than that derived from the bi-spectral retrieval for two of the three cases. The absolute difference between the multispectral estimate of liquid water path and that derived from the bi-spectral method for Fig. 3a, 3b, and 3c are 1.5, 0.7, and 12.5 $g\ m^{-2}$, respectively. There are several factors contributing to these results. While the retrieval of the radius at cloud top was close to the in situ measurements in all cases, the retrieval of the radius at cloud bottom was consistently larger than the in situ measurement. Second, we showed in Fig. 2 that the median vertical profile of droplet size of over 100 in situ measurements was close to adiabatic. This provided the basis for assuming an adiabatic droplet profile in the forward model, but this does not mean all in situ measured profiles were adiabatic, as evidenced by the large spread in the observations.

https://doi.org/10.5194/egusphere-2025-546
Preprint. Discussion started: 13 February 2025

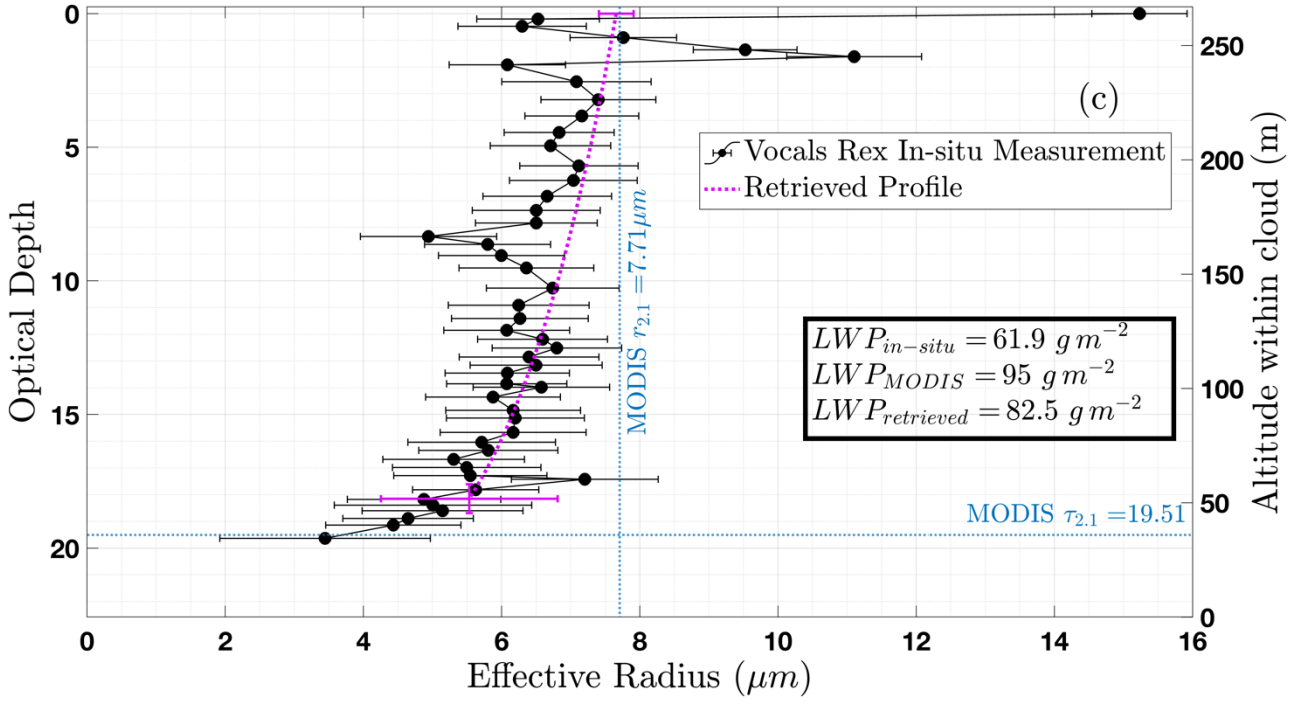

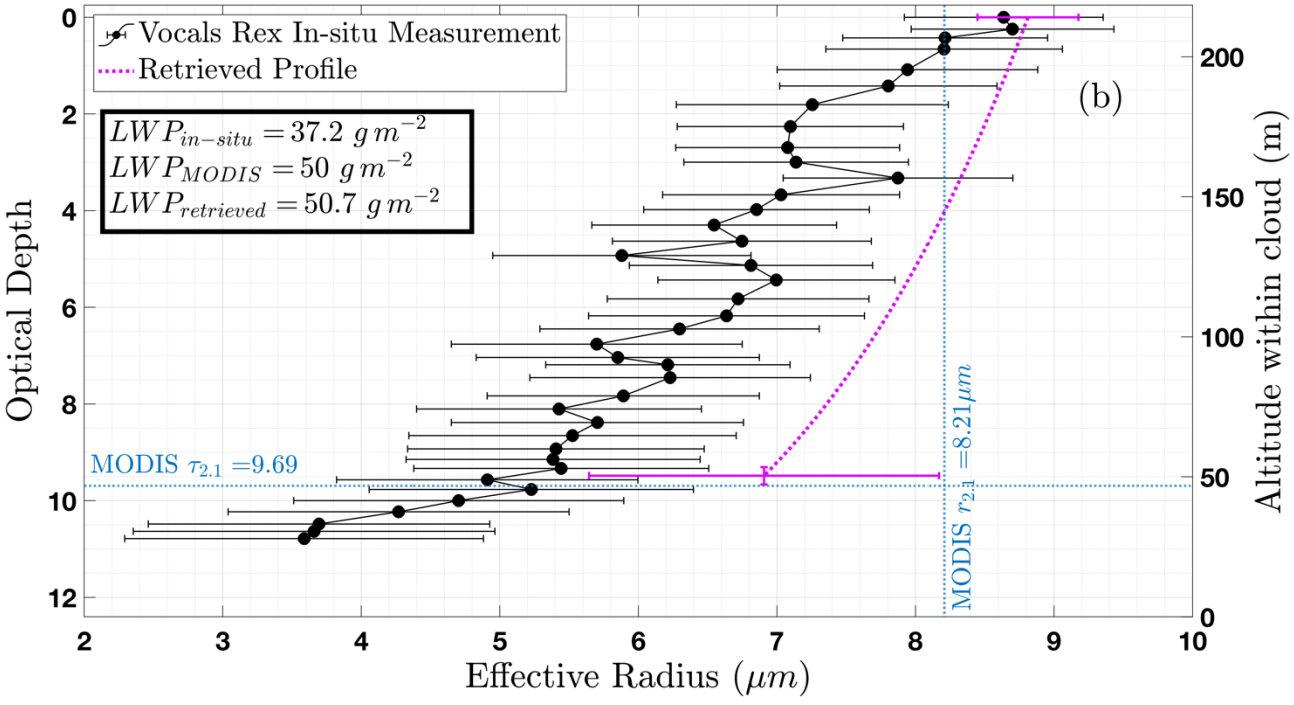

https://doi.org/10.5194/egusphere-2025-546
Preprint. Discussion started: 13 February 2025

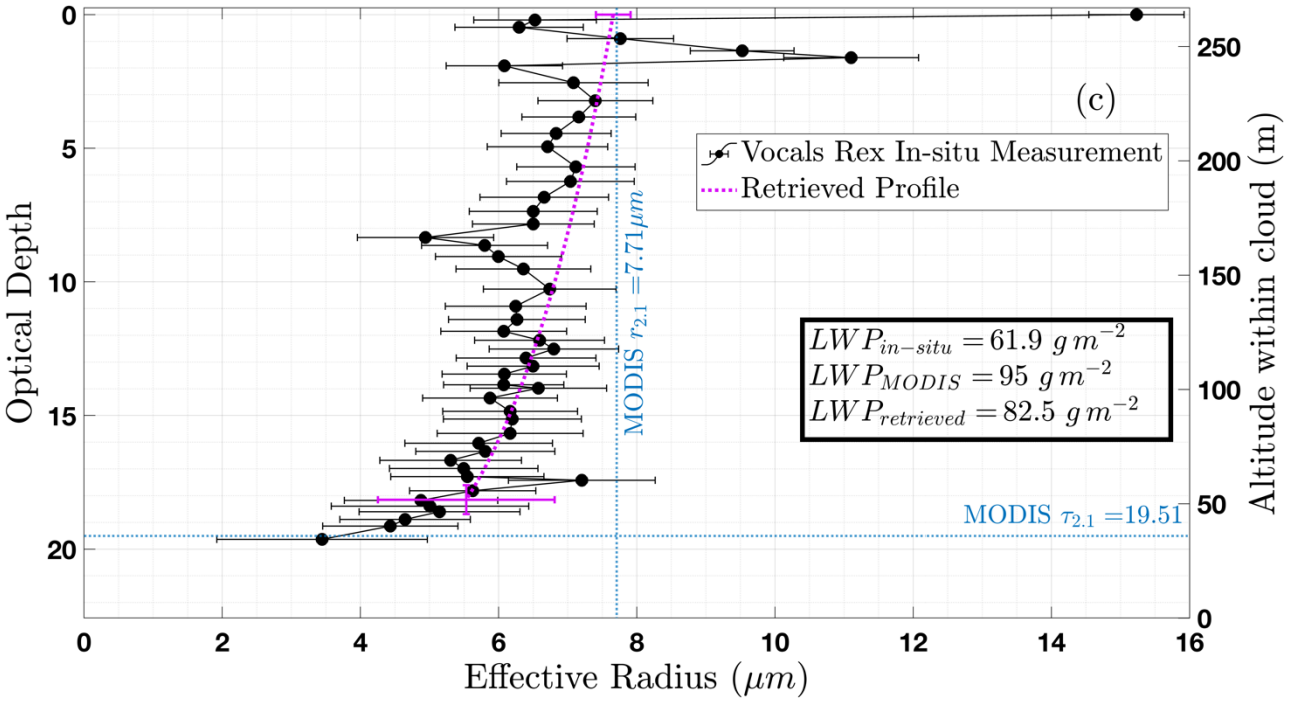

Figure 3: Comparison between effective radius calculated from in situ measurements (black circles), the MODIS bi-spectral retrieval of effective radius and optical depth (dotted vertical and horizonal blue lines, respectively), and the retrieved vertical profile using the constrained optimal estimation method (pink dashed line). The liquid water path estimate using in situ data, the MODIS retrievals, and our retrieved vertical profile are stated in the bolded box. Retrieval uncertainty for the effective radius at cloud top and bottom are shown as pink horizontal bars. In situ uncertainties are shown as black horizontal bars. MODIS and in situ data recorded on (a) 11 Nov., 2008, (b) and (c) 9 Nov., 2008

The retrieved droplet profiles in Fig 3a and 3b follow a similar pattern to their respective in situ measurements, but both are larger than the in situ at nearly all levels within the cloud. This clearly affects the liquid water path comparisons. In particular, the retrieved effective radius at cloud base in Fig. 3b did not match the in situ measurements as well as the other two cases. As such, the estimated liquid water path using the retrieved profile was nearly identical to the value estimated by the bi-spectral retrieval. It proved difficult to determine exactly why this case fared worse than the other two, and it appears at odds with King and Vaughan (2012) who found uncertainty of the effective radius at cloud base to be at a minimum for a cloud optical depth of about 10 when using synthetic data.

We investigated the uniqueness of the retrieved solutions and found that the constraints applied to the Gauss-Newton technique outlined in Sect. 2.3 were required to retrieve droplet profiles that consistently resembled in situ measurements. The Gauss-Newton solver is not designed to find the global minimum. Instead, it converges towards a local minimum, which depends on the initial state vector estimate and the a priori (Rodgers, 2000). Indeed, there are many state vectors that will result in a set of spectral measurements within the MODIS measurement uncertainty because of the low relative weights near cloud base for

https://doi.org/10.5194/egusphere-2025-546
Preprint. Discussion started: 13 February 2025

the seven spectral channels used in this analysis. In our analysis we found that without constraints on the solution space, even an a priori close to the in situ values for the radius at cloud top and bottom could still lead to a solution with $r_{top} < r_{bot}$, which invalidated the forward model assumptions.

To provide insight into the sensitivity of the multispectral retrieval of r_{bot} with cloud optical depth we analyzed the components of the Jacobian. Figure 4 shows the change in estimated spectral reflectance, $R(\boldsymbol{x}_i)$, due to a change in the cloud bottom radius for three clouds with differing values of optical depth. The behavior observed in Fig. 4 matches our expectations defined by the bi-spectral method. The change in estimated reflectance due to a change in r_{bot} is small in the visible where the droplet single scattering albedo is close to 1. In the near-infrared, water droplet absorption is proportional to the droplet radius. Thus, we expected a greater change in reflectance in the near-infrared spectral channels as the cloud bottom radius increases due to decreasing single scattering albedo. However, as optical depth increased, fewer photons penetrated the cloud's full depth, and eventually there was no change in reflectance.

The black circles in Fig. 4 shows the measurement uncertainty for the MODIS channels. For moderately thin clouds with an optical depth of less than 10, the change in reflectance typically exceeds the measurement uncertainty at wavelengths 1.64 μm and 2.13 μm. Changes in estimated reflectance when optical depth was 20 were equivalent or less than the measurement uncertainty. This represents an upper threshold in optical depth over which this retrieval is valid. Figure 4 also emphasizes expected improvements in this method from utilizing CPF measurements with radiometric uncertainty of 0.3% (Shea et al., 2020).

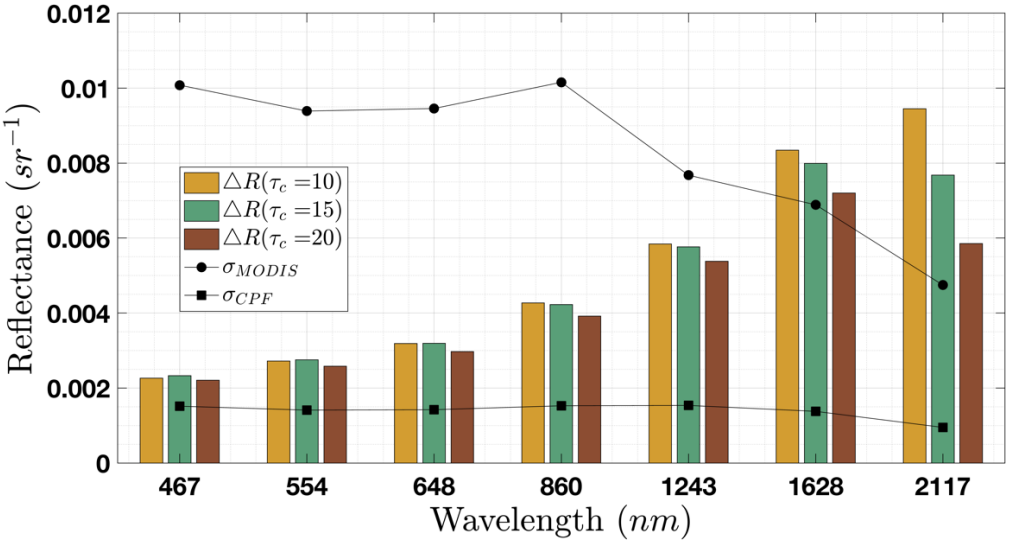

Figure 4: The change in our estimate of spectral reflectance due to a change in r_{bot}. The black circles show the MODIS measurement uncertainty in reflectance for each spectral channel. Three different cloud optical depths were compared to determine optical depth limits. The black squares show the measurement uncertainty for CPF is below the change in reflectance for each spectral channel.

https://doi.org/10.5194/egusphere-2025-546
Preprint. Discussion started: 13 February 2025

435

4.1 Comparing in situ measurements with remote retrievals

It is important to acknowledge the difficulty in comparing remote retrievals of droplet size with their in situ measured counterparts. We used the in situ measurements as a guide while developing our algorithm, but it would be incorrect to treat
440 them as absolute truth. At nadir, the area sampled on the ground by a single MODIS pixel is 1 km^2. With a near-circular orbit, the Terra and Aqua satellites have a roughly constant height above Earth's surface of about 709 km. We estimate the sampling volume of a plane parallel cloud with a 0.5 km thickness viewed by a single nadir-looking pixel to be about 0.167 km^3. The sampling volume of the CDP laser probe is the product of the distance traveled by the plane over the sampling time with the sampling area of the instrument, which is about 0.3 mm^2 (Lance et al., 2010). The C130 aircraft that carried the CDP flew at
445 an average speed of 107 $m\ s^{-1}$. With a 1 Hz sampling rate, the sampling volume of the CDP instrument was about 32 cm^3, or $3.2 \cdot 10^{-14}\ km^3$. Therefore, the volumes sampled by the aircraft instruments and the MODIS spectrometer differ by 13 orders of magnitude. The enormous difference requires a discussion about the spatial variability of droplet size within marine stratocumulus clouds.

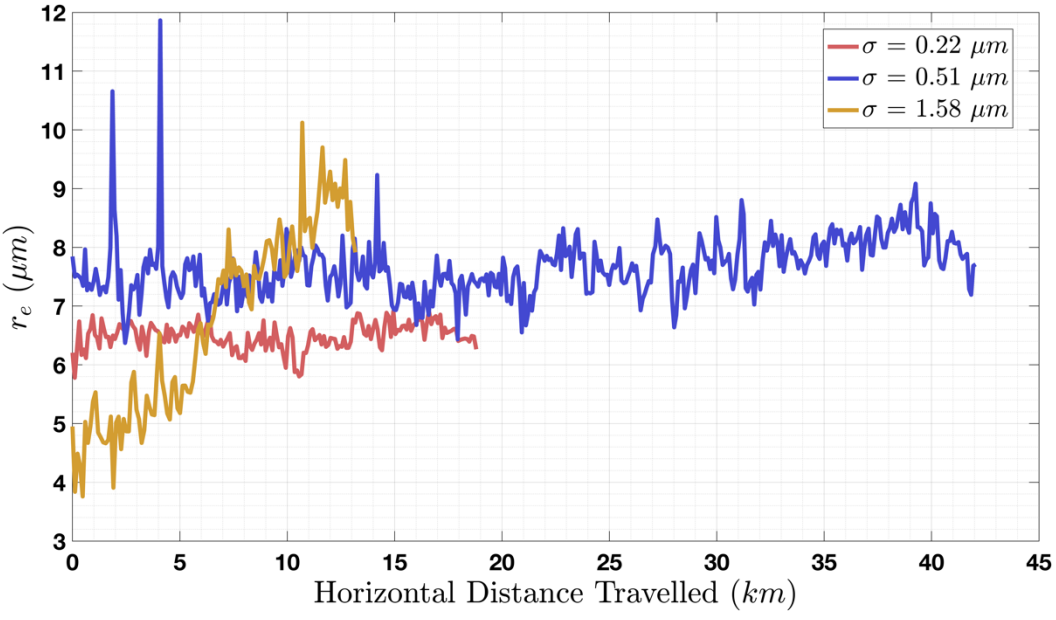

450 **Figure 5: Three horizontal profiles of effective radius from three different non-precipitating marine stratus clouds. These measurements were made at a near-constant altitude during the VOCALS-Rex field campaign on 9 Nov. 2008. The standard deviations of effective radius over each profile are shown in the legend.**

Throughout the VOCALS-Rex flight campaign, numerous horizontal flight paths were conducted at a near-constant altitude. We used these profiles to investigate the horizontal variability of effective radius in non-precipitating clouds. Figure 5 shows
455 three representative horizontal profiles of effective droplet radius with a maximum vertical displacement during sampling of 10 m. The three shown in Fig. 5 are representative of the two common regimes of behavior: steadily increasing or decreasing,

https://doi.org/10.5194/egusphere-2025-546
Preprint. Discussion started: 13 February 2025

and a quasi-stable mean. The range of these three horizontal profiles conveys how much change in droplet size is possible. These ranges were calculated to be 1.1 μm (red), 5.5 μm (blue), and 6 (yellow) μm.

Using 50 horizontal in situ profiles from VOCALS-REx, we computed the standard deviation of effective radius over two spatial scales representing the smallest and largest cross-track MODIS pixel sampling distances on the ground. At nadir, the cross-track sampling distance is 1 km, and at a scan angle of 55°, it is about 5 km long (Nishihama et al., 1997). We computed the standard deviation of droplet size over each length-scale by sliding windows equal to both length scales over all 50 horizontal profiles assuming the variability was invariant with direction within the horizontal plane. Figure 6 shows the histogram of standard deviations for the two length scales. The median variability for the 1 km length scale was 0.47 μm, whereas the median variability for the 5 km length scale was 0.56 μm. Thus, as scan angle increases, the pixel ground sampling area captures larger variations in droplet size.

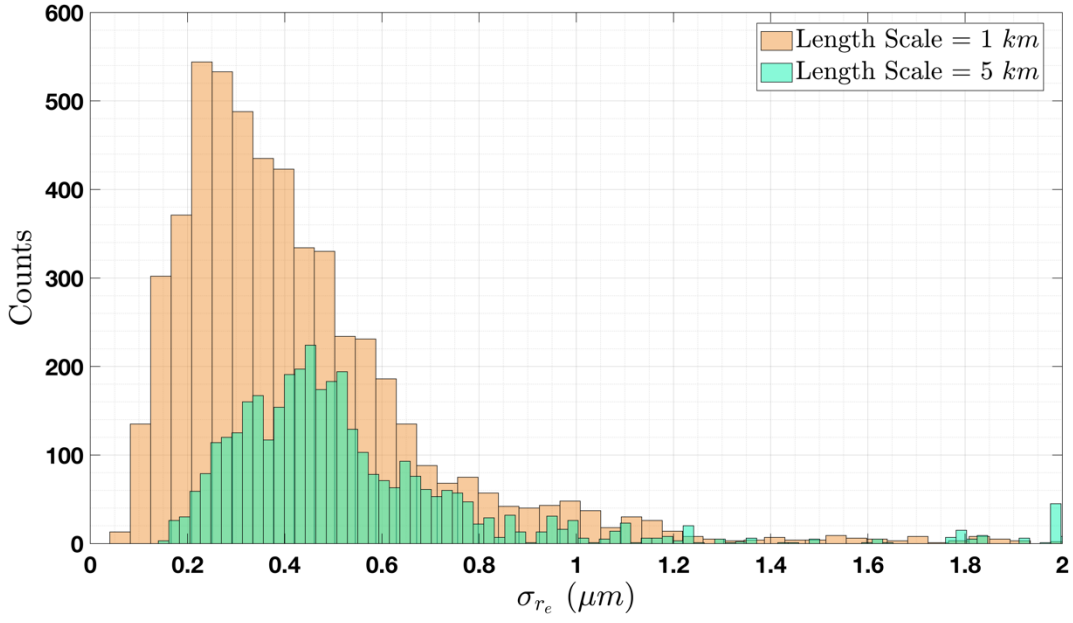

Figure 6: Histograms of the standard deviation of effective radius using horizontal profiles of non-precipitating clouds from the VOCALS-REx flight campaign. The standard deviations were calculated over the two along-scan pixel length extremes.

For comparing remote sensing with in situ measurements, it is important to recognize that the in situ profile represents a very small portion of the MODIS sampling volume. The retrieval of droplet size from MODIS measured radiance over a single pixel represents an integral over the sampled volume, which accounts for the contribution to reflectance at a given time, depth, and horizontal location (Feingold et al., 2006). In addition to the retrieval and in situ measurement uncertainties, the horizontal variability of droplet size is another ambiguity to consider when comparing remote retrievals with in-situ measurements.

https://doi.org/10.5194/egusphere-2025-546
Preprint. Discussion started: 13 February 2025

It should be noted that our classification of horizontal and vertical profiles is non-ideal but a necessary byproduct of airborne sampling. Every vertical profile sampled by VOCALS-REx spanned far more horizontal distance than vertical. Our intention with Fig. 2 was to show a representation of the distribution of droplet sizes sampled along the vertical dimension of a cloud; however, droplet horizontal variability is inevitably part of airborne vertical sampling.

Temporal variability also contributes to a discrepancy between in situ measurements and retrievals. The three vertical profiles shown in this paper are those closest in time between a MODIS and in situ measurement for the entire VOCALS-Rex field campaign. The time differences are 3.4 (Fig. 3a), 1.5 (Fig. 3b), and 4 minutes (Fig. 3c). We attempted to account for advection within our retrieval algorithm, but this does not account for the variability of cloud droplet size over time.

4.2 Simulated EMIT Spectra

We retrieved droplet profiles using the lookup table method introduced in Sect. 2.1 with simulated EMIT spectra to investigate two aspects that impact the solution space: the number of wavelengths used in the retrieval and the measurement uncertainty. Simulated reflectance spectra were generated in a similar manner to the synthetic data generated by King and Vaughan (2012). libRadtran was used to compute top-of-atmosphere reflected radiance spectra for plane-parallel clouds over ocean with an adiabatic droplet profile using 1D DISORT (Emde et al., 2016; Stamnes et al., 2000). Reflectance at each EMIT spectral channel was estimated by convolving the radiance spectrum with the EMIT spectral response functions and normalizing with the incident solar flux. Since we were unable to verify EMIT systematic and random uncertainty, we generated simulated spectra with varying uncertainty by sampling from a Gaussian distribution with zero mean. The lookup table method took about 50 times longer to compute than the iterative Gauss-Newton method, but once completed, we created a map from state space to measurement space. We repeated this process for different sets of spectral channels and for different values of measurement uncertainty in order to study how these two aspects affect the retrieval of droplet size at cloud base.

To quantify how the number of spectral channels used in the retrieval affects the solution, we solved for the state vector with two different sets of wavelengths. We modeled a cloudy scene off the coast of Chile using solar-viewing geometry from an EMIT measurement recorded on 17 January 2024, the same region where the VOCALS-REx field campaign took place in 2008 (Wood et al., 2011). The simulated reflectances were computed with 2% measurement uncertainty, the same value as the MODIS L1B reflectance uncertainty. Forward modeled reflectance was computed for different combinations of the three state variables, $\boldsymbol{x} = (r_{top}, r_{bot}, \tau_c)$. Figure 7 shows the contours of the relative residual, the fraction of the residual with respect to the ℓ^2-norm of the measurement uncertainty: $\sqrt{\sum(R(\boldsymbol{x}_i) - \boldsymbol{m})^2} / \sqrt{\sum(\delta \boldsymbol{m})^2}$. The left side of Fig. 7 was generated using seven spectral channels aligned with the seven MODIS spectral channels used in the multispectral retrieval (Table 1). The right side of Fig. 7 was generated using 35 spectral channels across the visible and near-infrared that avoided water vapor and other

https://doi.org/10.5194/egusphere-2025-546
Preprint. Discussion started: 13 February 2025

gaseous absorption. According to the convergence criteria outlined in Sect. 2.3, the iterative algorithm terminates when the residual is less than or equal to the ℓ^2-norm of the measurement uncertainty (Eq. (12)). This region of residual minima is located within the isopleth of one. State vectors within this isopleth lead to forward model reflectances within the uncertainty of the measurements. The solution space occupies three dimensions corresponding to the three retrieved variables. Figure 7 collapses the solution space into two dimensions by taking the difference between the cloud bottom radius dimension and the radius at cloud top associated with the global minimum relative residual. When we increased the number of spectral bands from seven to 35, the region of residual minima decreased along the cloud bottom radius dimension by about 2 μm. Furthermore, Fig. 7 demonstrates that when using 35 spectral channels with 2% measurement uncertainty, state vectors within the isopleth of one do not include any droplet profiles with a larger radius at cloud bottom than cloud top, represented by negative values on the y-axis.

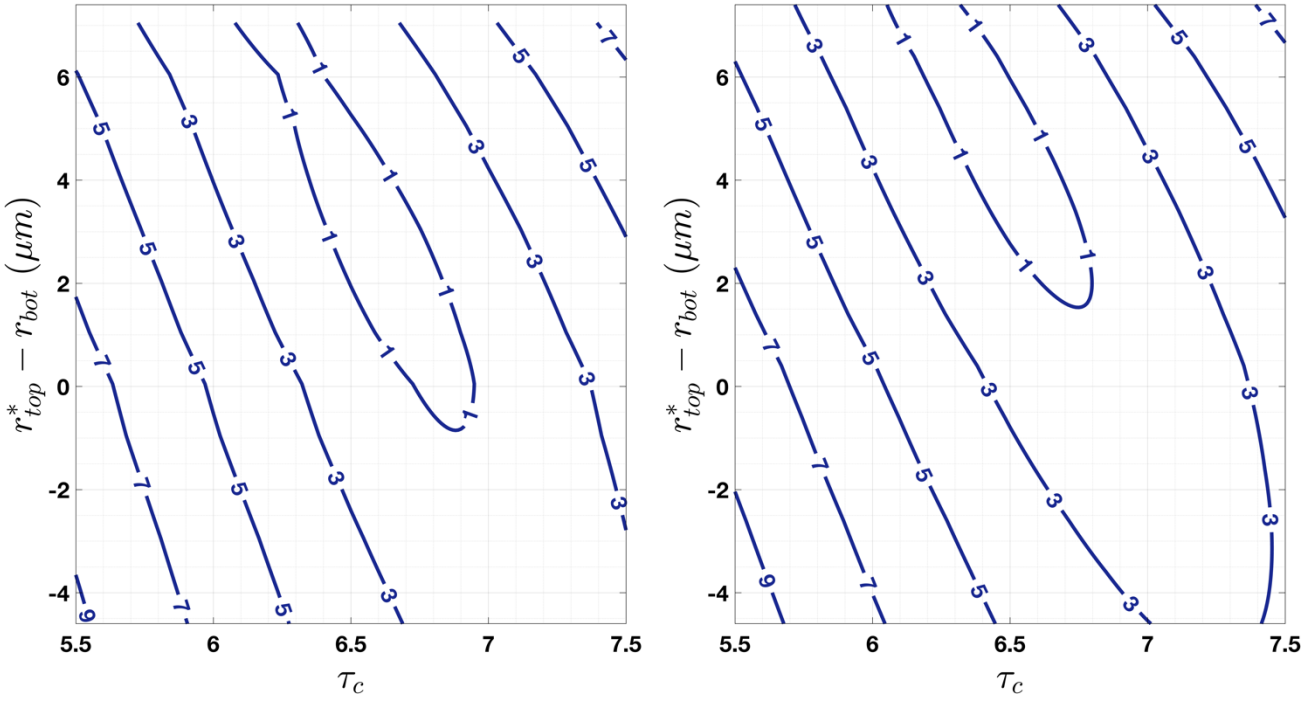

Figure 7: Contours of the relative ℓ^2-norm difference between the libRadtran-estimated reflectance and simulated EMIT spectra. The left panel was generated using 7 spectral channels that align with those used in the multispectral retrieval in Sect. 4.1 and the right panel with 35 spectral channels throughout the visible and near-infrared. The y-axis is the difference between the cloud top radius value associated with the global minimum relative ℓ^2-norm and the cloud bottom radius. The x-axis varies with cloud optical depth.

Figure 8 demonstrates how measurement uncertainty affects the solution space. We computed forward modeled reflectances for the same scene described above for Fig. 7, but we kept the number of wavelengths used in the retrieval constant, using the same 35 spectral channels as the right side of Fig. 7. The left side of Fig. 8 shows the relative residual using synthetic spectra with 2% measurement uncertainty, whereas the right applied a 0.3% measurement uncertainty, similar to the value reported

https://doi.org/10.5194/egusphere-2025-546
Preprint. Discussion started: 13 February 2025

for the upcoming CPF instrument (Shea et al., 2020). Unlike the modest reduction of the residual minima region with increasing wavelengths, Fig. 8 shows a significant reduction with decreasing measurement uncertainty. The region within the isopleth of one decreased along the cloud bottom radius dimension by about 5 μm. It's important to note that the shape of the contours in Figs. 7 and 8 depends on the droplet profile of the cloud and varies with each simulated EMIT spectra because of the addition of Gaussian noise. Both figures show the most common results from many simulations.

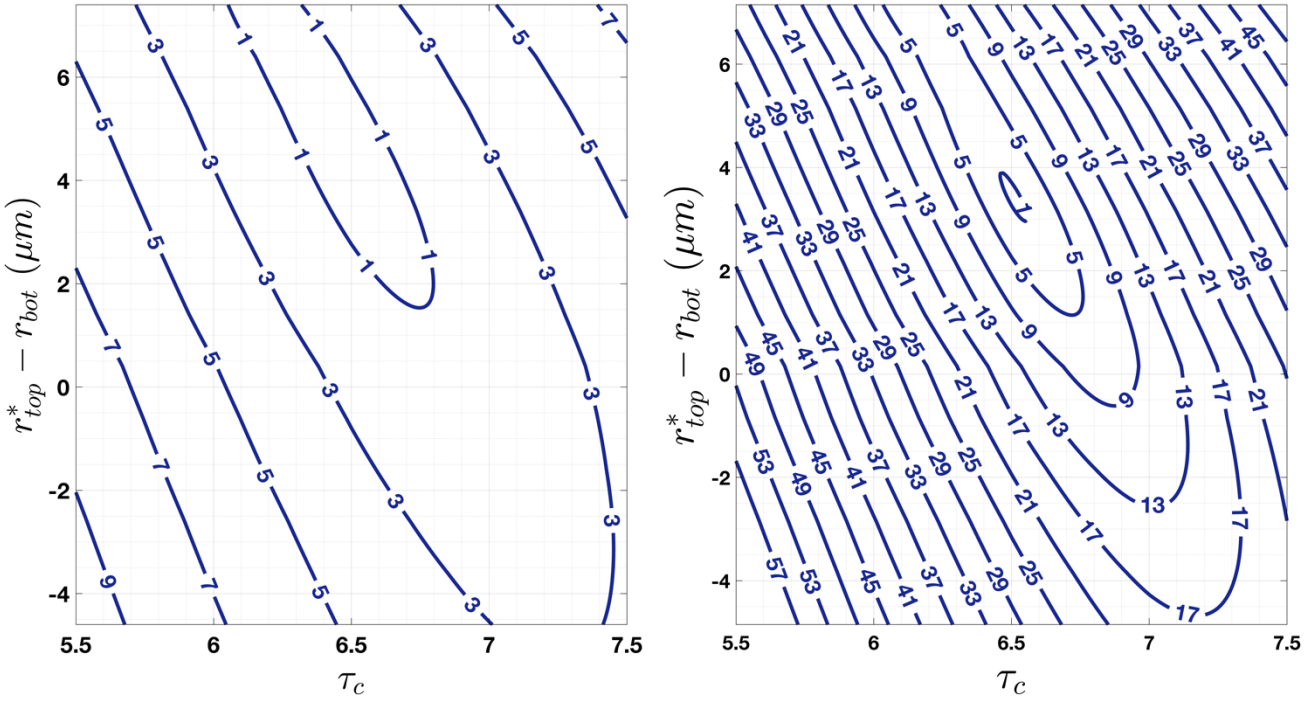

Figure 8: Contours of the relative ℓ^2-norm difference between the libRadtran-estimated reflectance and simulated EMIT spectra. The left and right panels used simulated EMIT reflectances with 2% and 0.3% measurement uncertainty, respectively. The y-axis is the difference between the cloud top radius value associated with the global minimum relative ℓ^2-norm, and the cloud bottom radius. The x-axis varies with cloud optical depth. Both panels used 35 spectral channels throughout the visible and near-infrared.

5 Discussion and Conclusions

To prepare for upcoming high-accuracy, full-spectral space-borne hyperspectral measurements, we have developed new methods to retrieve vertical profiles of cloud droplet size. We extended the results of King and Vaughan (2012) by creating a constrained form of the iterative Gauss-Newton technique and applied it to real data. Using the first seven spectral channels of MODIS and coincident in situ measurements from the VOCALS-REx flight campaign, we showed that retrieving a profile of effective radius is possible, but solving for the effective radius at cloud base is problematic because of the similarity of weighting functions at various visible and near-infrared wavelengths. Other studies have retrieved vertical profiles of effective radius from MODIS data without addressing solution uniqueness (Chang and Li, 2003; Kokhanovsky and Rozanov, 2012).

https://doi.org/10.5194/egusphere-2025-546
Preprint. Discussion started: 13 February 2025

Chang and Li (2003) outlined methods to retrieve droplet profiles, applied these methods to real data, and investigated changes in retrieved variables due to reflectance uncertainty. Kokhanovsky and Rozanov (2012) used the Gauss-Newton optimal estimation method to retrieve droplet profiles, demonstrating that their method worked on real data. King and Vaughan (2012) investigated the impact of measurement uncertainty on retrieval uncertainty using synthetic data but did not address solution uniqueness. The limited unique information in the MODIS bands used in our analysis led to a non-unique solution, with many droplet profiles leading to a set of spectral measurements within the MODIS measurement uncertainty. We implemented a constrained form of the algorithm, which reduced the solution space to a set consistent with the forward model assumptions, leading to state vectors that more closely matched the in situ measurements.

Coincident in situ measurements were used to validate the retrieval. Algorithmic parameters described in Sect. 2.3 were tuned such that the retrieved droplet profile closely matched the in situ measurements. However, in situ measurements cannot be treated as absolute truth because the sampling volumes of VOCALS-REx and the MODIS measurements differ by 13 orders of magnitude. Using VOCALS-REx in situ data, we found the median horizontal variability of effective radius to be between 0.47 μm and 0.56 μm for the two extremes of the MODIS along-scan pixel ground sampling distances of 1 and 5 km. These values were small but nonetheless, affect the comparison between in situ measurements and remote retrievals. The retrieved droplet size is representative of a radiatively-weighted mean over the sampling volume. The in situ measurement is considered a point measurement, which is more susceptible to spatial perturbations. Horizontal variability of effective radius over the MODIS pixel sampling area should be taken into account, along with the in situ measurement and retrieval uncertainty, when making these comparisons.

All three in situ vertical profiles analyzed in this paper spanned multiple MODIS pixels. Unfortunately, there was never a scenario where a vertical profile was completely contained within a single pixel. We found that the overlapping pixel with an optical depth closest to the in situ measurement performed best in the retrieval. This result demonstrates the important interdependence between the retrieved variables: we required an accurate a priori of optical depth to retrieve droplet sizes that more closely matched the in situ measurements. Indeed, Figs. 7 and 8 demonstrate the importance of an accurate a priori and initial guess because these values help define the approach to the convergence region. Future work will explore non-diagonal covariance matrices and the interdependence between the retrieved variables.

The first seven spectral channels of MODIS were used in this analysis because they avoid water vapor absorption. When we increased the number of wavelengths from seven to 35 using simulated EMIT spectra, we found that the region of residual minima within the solution space decreased along the cloud bottom radius dimension by about 2 μm. Future applications with hyperspectral measurements from EMIT and CPF will consider hundreds of spectral bands, including those in the wings of near-infrared water vapor absorption features. Perhaps this additional information will enhance the modest improvements to the retrieval of droplet size at cloud base shown in Fig. 7 by increasing the retrieval signal-to-noise ratio.

https://doi.org/10.5194/egusphere-2025-546
Preprint. Discussion started: 13 February 2025

The optical depth over which the droplet size at cloud base can be retrieved is limited by the uncertainty of the measurements. Changes in the spectral reflectance due to a change in droplet size at cloud base were often below the MODIS measurement uncertainty for optically thick clouds. Figure 4 illustrates that CPF measurement uncertainty, which is lower than the estimated change in reflectance at every spectral channel used in this analysis, will improve the retrieval of droplet size at cloud base. Furthermore, Fig. 8 shows a 5 μm reduction in the region of residual minima along the cloud bottom radius dimension when measurement uncertainty drops from 2% to 0.3%. These results underscore the importance of higher accuracy from the next generation of space-borne spectrometers. The results of this study suggest that a reduction in radiometric uncertainty is a more significant factor for retrieving droplet profiles than increasing the number of spectral bands.

Code and Data Availability. The retrieval algorithm developed for this paper is freely available on GitHub (https://github.com/andrewjbuggee/multispectral-retrieval-using-MODIS). The MODIS L1B reflectance data sets used for retrieving droplet profiles are described within the previously mentioned GitHub repository and freely available at NASA's Level-1 and Atmosphere Archive & Distribution System Distributed Active Archive Center (LAADS-DAAC): https://ladsweb.modaps.eosdis.nasa.gov/. The VOCALS-REx data used for comparison with the multispectral retrievals are similarly defined within the GitHub repository. These data are maintained by the National Center for Atmospheric Research Earth Observing Laboratory Field Data Archive (NCAR EOL) and are freely available at: https://doi.org/10.5065/D60863M8.

Author Contributions. AJB led the study, developed the retrieval algorithm, and wrote the paper. PP made extensive paper edits and provided ideas, comments, and suggestions throughout the project.

Competing Interests. None of the authors of this paper have competing interests.

Acknowledgements. The authors would like to thank Dr. Odele Coddington, Dr. Kevin McGouldrick, and Dr. Zhien Wang for reading early drafts and providing feedback. Their comments significantly improved this project. This material is based upon work supported by the National Science Foundation Graduate Research Fellowship under Grant No. 2040434.

https://doi.org/10.5194/egusphere-2025-546
Preprint. Discussion started: 13 February 2025

References

Amarasinghe, N., Platnick, S., and Meyer, K.: Overview of the MODIS Collection 6 Cloud Optical Property (MOD06) Retrieval Look-up Tables, 2017.

Bohren, C. F. and Clothiaux, E. E.: Fundamentals of Atmospheric Radiation, Wiley-VCH, Darmstadt, 2006.

Chang, F. L. and Li, Z.: Estimating the vertical variation of cloud droplet effective radius using multispectral near-infrared satellite measurements, Journal of Geophysical Research Atmospheres, 107, 1–12, 2002.

Chang, F.-L. and Li, Z.: Retrieving vertical profiles of water-cloud droplet effective radius: Algorithm modification and preliminary application, Journal of Geophysical Research: Atmospheres, 108, https://doi.org/10.1029/2003JD003906, 2003.

Chen, R., Chang, F.-L., Li, Z., Ferraro, R., and Weng, F.: Impact of the Vertical Variation of Cloud Droplet Size on the Estimation of Cloud Liquid Water Path and Rain Detection, Journal of the Atmospheric Sciences, 64, 3843–3853, https://doi.org/10.1175/2007JAS2126.1, 2007.

Coddington, O., Pilewskie, P., and Vukicevic, T.: The Shannon information content of hyperspectral shortwave cloud albedo measurements: Quantification and practical applications, Journal of Geophysical Research Atmospheres, 117, 1–12, https://doi.org/10.1029/2011JD016771, 2012.

Deirmendjian, D.: Scattering and Polarization Properties of Water Clouds and Hazes in the Visible and Infrared, Appl. Opt., 3, 187, https://doi.org/10.1364/AO.3.000187, 1964.

Doicu, A., Schreier, F., and Hess, M.: Iteratively regularized Gauss–Newton method for bound-constraint problems in atmospheric remote sensing, Computer Physics Communications, 153, 59–65, https://doi.org/10.1016/S0010-4655(03)00138-3, 2003.

Emde, C., Buras-Schnell, R., Kylling, A., Mayer, B., Gasteiger, J., Hamann, U., Kylling, J., Richter, B., Pause, C., Dowling, T., and Bugliaro, L.: The libRadtran software package for radiative transfer calculations (version 2.0.1), Geoscientific Model Development, 9, 1647–1672, https://doi.org/10.5194/gmd-9-1647-2016, 2016.

Feingold, G., Furrer, R., Pilewskie, P., Remer, L. A., Min, Q., and Jonsson, H.: Aerosol indirect effect studies at Southern Great Plains during the May 2003 Intensive Operations Period, Journal of Geophysical Research Atmospheres, 111, https://doi.org/10.1029/2004JD005648, 2006.

Green, R. O., Mahowald, N., Ung, C., Thompson, D. R., Bator, L., Bennet, M., Bernas, M., Blackway, N., Bradley, C., Cha, J., Clark, P., Clark, R., Cloud, D., Diaz, E., Ben Dor, E., Duren, R., Eastwood, M., Ehlmann, B. L., Fuentes, L., Ginoux, P., Gross, J., He, Y., Kalashnikova, O., Kert, W., Keymeulen, D., Klimesh, M., Ku, D., Kwong-Fu, H., Liggett, E., Li, L., Lundeen, S., Makowski, M. D., Mazer, A., Miller, R., Mouroulis, P., Oaida, B., Okin, G. S., Ortega, A., Oyake, A., Nguyen, H., Pace, T., Painter, T. H., Pempejian, J., Garcia-Pando, C. P., Pham, T., Phillips, B., Pollock, R., Purcell, R., Realmuto, V., Schoolcraft, J., Sen, A., Shin, S., Shaw, L., Soriano, M., Swayze, G., Thingvold, E., Vaid, A., and Zan, J.: The Earth Surface Mineral Dust Source Investigation: An Earth Science Imaging Spectroscopy Mission, in: 2020 IEEE Aerospace Conference, 2020 IEEE Aerospace Conference, 1–15, https://doi.org/10.1109/AERO47225.2020.9172731, 2020.

Hansen, J. E. and Pollack, J. B.: Near-Infrared Light Scattering by Terrestrial Clouds, Journal of the Atmospheric Sciences, 27, 265–281, 1970.

Hansen, J. E. and Travis, L. D.: Light Scattering in Planetary Atmospheres, Space Science Reviews, 16, 527–610, 1974.

https://doi.org/10.5194/egusphere-2025-546
Preprint. Discussion started: 13 February 2025

King, M. D., Kaufman, Y. J., Menzel, W. P., and Tanre, D.: Remote sensing of cloud, aerosol, and water vapor properties from the moderate resolution imaging spectrometer (MODIS), IEEE Trans. Geosci. Remote Sensing, 30, 2–27, https://doi.org/10.1109/36.124212, 1992.

King, N. J. and Vaughan, G.: Using passive remote sensing to retrieve the vertical variation of cloud droplet size in marine stratocumulus: An assessment of information content and the potential for improved retrievals from hyperspectral measurements, Journal of Geophysical Research Atmospheres, 117, https://doi.org/10.1029/2012JD017896, 2012.

King, N. J., Bower, K. N., Crosier, J., and Crawford, I.: Evaluating modis cloud retrievals with in situ observations from VOCALS-REx, Atmospheric Chemistry and Physics, 13, 191–209, https://doi.org/10.5194/acp-13-191-2013, 2013.

Kokhanovsky, A. and Rozanov, V. V.: Droplet vertical sizing in warm clouds using passive optical measurements from a satellite, Atmospheric Measurement Techniques, 5, 517–528, https://doi.org/10.5194/amt-5-517-2012, 2012.

Lance, S., Brock, C. A., Rogers, D., and Gordon, J. A.: Water droplet calibration of the Cloud Droplet Probe (CDP) and in-flight performance in liquid, ice and mixed-phase clouds during ARCPAC, Atmospheric Measurement Techniques, 3, 1683–1706, https://doi.org/10.5194/amt-3-1683-2010, 2010.

Miles, N. L., Verlinde, J., and Clothiaux, E. E.: Cloud droplet size distributions in low-level stratiform clouds, Journal of the Atmospheric Sciences, 57, 295–311, https://doi.org/10.1175/1520-0469(2000)057<0295:CDSDIL>2.0.CO;2, 2000.

Miller, D. J., Zhang, Z., Ackerman, A. S., Platnick, S., and Baum, B. A.: The impact of cloud vertical profile on liquid water path retrieval based on the bispectral method: A theoretical study based on large-eddy simulations of shallow marine boundary layer clouds, Journal of Geophysical Research: Atmospheres, 121, 4122–4141, https://doi.org/10.1002/2015JD024322, 2016.

Nakajima, T. and King, M. D.: Determination of the optical thickness and effective particle radius of clouds from reflected solar radiation measurements. Part I: Theory., Journal of Atmospheric Sciences, 47, 1878–1893, 1990.

Nakajima, T., King, M., Spinhirne, J., and Radke, L.: Determination of the Optical-Thickness and Effective Particle Radius of Clouds from Reflected Solar-Radiation Measurements .2. Marine Stratocumulus Observations, J. Atmos. Sci., 48, 728–750, https://doi.org/10.1175/1520-0469(1991)048<0728:DOTOTA>2.0.CO;2, 1991.

Nishihama, M., Wolfe, R., Solomon, D., Patt, F., Blanchette, J., Fleig, A., and Masuoka, E.: MODIS L1A Earth Location Algorithm Theoretical Basis Document Version 3.0, 1997.

Painemal, D. and Zuidema, P.: Assessment of MODIS cloud effective radius and optical thickness retrievals over the Southeast Pacific with VOCALS-REx in situ measurements, Journal of Geophysical Research Atmospheres, 116, 1–16, https://doi.org/10.1029/2011JD016155, 2011.

Pilewskie, P. and Twomey, S.: Discrimination of ice from water in clouds by optical remote sensing, Atmospheric Research, 21, 113–122, https://doi.org/10.1016/0169-8095(87)90002-0, 1987.

Platnick, S.: Vertical photon transport in cloud remote sensing problems, Journal of Geophysical Research Atmospheres, 105, 22919–22935, https://doi.org/10.1029/2000JD900333, 2000.

Platnick, S. and Valero, F. P. J.: A Validation of a Satellite Cloud Retrieval during ASTEX, 1995.

Platnick, S., King, M. D., Ackerman, S. A., Menzel, W. P., Baum, B. A., Riédi, J. C., and Frey, R. A.: The MODIS cloud products: Algorithms and examples from terra, IEEE Transactions on Geoscience and Remote Sensing, 41, 459–472, https://doi.org/10.1109/TGRS.2002.808301, 2003.

https://doi.org/10.5194/egusphere-2025-546
Preprint. Discussion started: 13 February 2025

Platnick, S., Meyer, K. G., King, M. D., Wind, G., Amarasinghe, N., Marchant, B., Arnold, G. T., Zhang, Z., Hubanks, P. A., Holz, R. E., Yang, P., Ridgway, W. L., and Riedi, J.: The MODIS Cloud Optical and Microphysical Products: Collection 6 Updates and Examples from Terra and Aqua, IEEE Transactions on Geoscience and Remote Sensing, 55, 502–525, https://doi.org/10.1109/TGRS.2016.2610522, 2017.

Rodgers, C. D.: Inverse Methods for Atmospheric Souding: Theory and Practice, 2000.

Sagan, C. and Pollack, J. B.: Anisotropic nonconservative scattering and the clouds of Venus, Journal of Geophysical Research, 72, 469–477, https://doi.org/10.1029/jz072i002p00469, 1967.

Shea, Y., Fleming, G., Kopp, G., Lukashin, C., Pilewskie, P., Smith, P., Thome, K., Wielicki, B., Liu, X., and Wu, W.: Clarreo Pathfinder: Mission Overview and Current Status, International Geoscience and Remote Sensing Symposium (IGARSS), 4, 3286–3289, https://doi.org/10.1109/IGARSS39084.2020.9323176, 2020.

Stamnes, K., Tsay, S.-C., Wiscombe, W., and Laszlo, I.: DISORT, a General-Purpose Fortran Program for Discrete-Ordinate-Method Radiative Transfer in Scattering and Emitting Layered Media: Documentation of Methodology, 2000.

Stephens, G. L.: Cloud feedbacks in the climate system: A critical review, Journal of Climate, 18, 237–273, https://doi.org/10.1175/JCLI-3243.1, 2005.

Stephens, G. L. and Tsay, S.-C.: On the cloud absorption anomaly, Quarterly Journal of the Royal Meteorological Society, 116, 671–704, https://doi.org/10.1002/qj.49711649308, 1990.

Stephens, G. L., Christensen, M., Andrews, T., Haywood, J., Malavelle, F. F., Suzuki, K., Jing, X., Lebsock, M., Li, J. L. F., Takahashi, H., and Sy, O.: Cloud physics from space, Quarterly Journal of the Royal Meteorological Society, 145, 2854–2875, https://doi.org/10.1002/qj.3589, 2019.

Strapp, J. W., Albers, F., Reuter, A., Korolev, A. V., Maixner, U., Rashke, E., and Vukovic, Z.: Laboratory Measurements of the Response of a PMS OAP-2DC, Journal of Atmospheric and Oceanic Technology, 18, 1150–1170, 2001.

Thompson, D. R., Green, R. O., Bradley, C., Brodrick, P. G., Mahowald, N., Dor, E. B., Bennett, M., Bernas, M., Carmon, N., Chadwick, K. D., Clark, R. N., Coleman, R. W., Cox, E., Diaz, E., Eastwood, M. L., Eckert, R., Ehlmann, B. L., Ginoux, P., Ageitos, M. G., Grant, K., Guanter, L., Pearlshtien, D. H., Helmlinger, M., Herzog, H., Hoefen, T., Huang, Y., Keebler, A., Kalashnikova, O., Keymeulen, D., Kokaly, R., Klose, M., Li, L., Lundeen, S. R., Meyer, J., Middleton, E., Miller, R. L., Mouroulis, P., Oaida, B., Obiso, V., Ochoa, F., Olson-Duvall, W., Okin, G. S., Painter, T. H., Pérez García-Pando, C., Pollock, R., Realmuto, V., Shaw, L., Sullivan, P., Swayze, G., Thingvold, E., Thorpe, A. K., Vannan, S., Villarreal, C., Ung, C., Wilson, D. W., and Zandbergen, S.: On-orbit calibration and performance of the EMIT imaging spectrometer, Remote Sensing of Environment, 303, 113986, https://doi.org/10.1016/j.rse.2023.113986, 2024.

Twomey, S. and Bohren, C. F.: Simple Approximations for Calculations of Absorption in Clouds, Journal of Atmospheric Sciences, 37, 2086–2094, 1980.

Twomey, S. and Cocks, T.: Spectral Reflectance of Clouds Comparison of Measurements in the and Calculations By S . Twomey Institute of Atmospheric Physics , the University of Arizona , Tucson , Ariz . 85721 T . Cocks Division of Cloud Physics , Commonwealth Scientific and Industri, 1982.

Twomey, S. and Seton, K. J.: Inferences of Gross Microphysical Properties of Clouds from Spectral Reflectance Measurements, Journal of Atmospheric Sciences, 37, 1065–1069, 1980.

https://doi.org/10.5194/egusphere-2025-546
Preprint. Discussion started: 13 February 2025

Wood, R., Mechoso, C. R., Bretherton, C. S., Weller, R. A., Huebert, B., Straneo, F., Albrecht, B. A., Coe, H., Allen, G., Vaughan, G., Daum, P., Fairall, C., Chand, D., Gallardo Klenner, L., Garreaud, R., Grados, C., Covert, D. S., Bates, T. S., Krejci, R., Russell, L. M., De Szoeke, S., Brewer, A., Yuter, S. E., Springston, S. R., Chaigneau, A., Toniazzo, T., Minnis, P., Palikonda, R., Abel, S. J., Brown, W. O. J., Williams, S., Fochesatto, J., Brioude, J., and Bower, K. N.: The VAMOS ocean-cloud-atmosphere-land study regional experiment (VOCALS-REx): Goals, platforms, and field operations, Atmospheric Chemistry and Physics, 11, 627–654, https://doi.org/10.5194/acp-11-627-2011, 2011.

Yau, M. K. and Rogers, R. R.: A Short Course in Cloud Physics, Elsevier, 308 pp., 1996.